blood®
Regular Article

RED CELLS, IRON, AND ERYTHROPOIESIS

Iron overload damages mitochondria and induces metabolic rewiring of hematopoietic stem cells toward glycolysis

Silvia Sighinolfi,[1] Laura Cassina,[2] Maria Rosa Lidonnici,[1] Stefano Beretta,[1] Davide Stefanoni,[2] Mariangela Storto,[1] Christina Mayerhofer,[3-5] Trine A. Kristiansen,[3-5] David T. Scadden,[3-5] Ivan Merelli,[1,6] Alessandra Boletta,[2] Annamaria Aprile,[1,*] and Giuliana Ferrari[1,7,*]

[1]San Raffaele Telethon Institute for Gene Therapy and [2]Division of Genetics and Cell Biology, Istituto di Ricovero e Cura a Carattere Scientifico San Raffaele Scientific Institute, Milan, Italy; [3]Center for Regenerative Medicine, Massachusetts General Hospital, Boston, MA; [4]Department of Stem Cell and Regenerative Biology, Harvard University, Cambridge, MA; [5]Harvard Stem Cell Institute, Cambridge, MA; [6]Institute for Biomedical Technologies, National Research Council, Segrate, Italy; and [7]Vita-Salute San Raffaele University, Milan, Italy

KEY POINTS

- **IO damages mitochondria and rewires HSC metabolism from oxidative phosphorylation to glycolysis.**
- **Targeting in vivo IO-derived mtROS rescues HSC defects in β-thalassemia.**

Iron is an essential element for most cellular processes, and recent evidence highlighted its role in regulating the function of hematopoietic stem cells (HSCs). Abnormal iron levels affect HSC quiescence and self-renewal; however, the mechanism by which iron overload (IO) influences HSC function is still unknown. Here, we show that intracellular IO impairs mitochondrial fitness and bioenergetics, inducing metabolic rewiring. In thalassemic mice, as a model of chronic IO, HSCs accumulate elevated mitochondrial reactive oxygen species (mtROS), low mitochondrial membrane potential, and reduced oxidative phosphorylation. Mitochondrial defects are confirmed in 2 other models of IO, sickle cell disease and iron-loaded wild-type mice, and in vivo iron reduction rescues HSC mitochondria. IO HSCs are highly proliferating and, in the presence of damaged mitochondria, rely on glycolysis for energy production. Notably, restoration of mitochondrial function by targeting in vivo mtROS improved the quiescence and self-renewal of IO HSCs. Our results unravel the critical interplay between iron, ROS, and mitochondrial activity in HSCs, revealing that IO shapes HSC metabolic programs.

Introduction

Hematopoietic stem cells (HSCs) sustain lifelong blood-cell formation.[1] At steady state, adult HSCs are maintained quiescent and divide rarely but they can reversibly exit from dormancy after exposure to several stimuli in the bone marrow (BM) to replenish the hematopoietic system.[2-4] A wide range of insults can perturb HSC function[5] through the accumulation of toxic molecules or reduced nutrient availability.[6] Among them, reactive oxygen species (ROS) within the physiological range drive HSC entry into the cell cycle, whereas their accumulation at higher levels results in oxidative damage of cellular organelles, and cell death.[7]

Iron is an essential element involved in several cellular processes, including oxygen transport, metabolism, DNA synthesis and repair, and cell signaling.[8] Iron exerts most of these functions as a cofactor of proteins in the form of iron-sulfur cluster and heme, including mitochondrial enzymes, and by participating in Fenton and Haber-Weiss reactions, which generate ROS.[9]

HSCs can import and accumulate iron from the microenvironment[10] and the maintenance of intracellular iron homeostasis guarantees the balance between self-renewal and differentiation. Both intracellular iron overload (IO) and intracellular iron deficiency induce HSC exhaustion through ROS generation, whereas physiological iron availability regulates HSC division during regeneration.[11-13] Limited intracellular iron content promotes mitochondrial fatty acid oxidation and epigenetic remodeling, thus resulting in increased HSC division.[10] However, the mechanisms by which IO is detrimental to HSC function are still largely unknown. Moreover, iron has been mostly studied in models of induced accumulation or deprivation and the knowledge about the role of iron on HSC function is still limited in disease context.[14]

Quiescent HSCs rely on anaerobic glycolysis and maintain a low mitochondrial metabolic activity in the BM niche. The transition to a more proliferative state associated with differentiation requires higher energy inputs, thus active HSCs enhance both glycolysis and oxidative phosphorylation (OXPHOS).[15,16] Mitochondria are the powerhouse of the cell,

in which OXPHOS takes place, and the continuous remodeling of the mitochondrial network through cycles of biogenesis, fusion, fission, and degradation through mitophagy, regulates HSC metabolism and function.[17] Recently, HSCs have been classified based on their mitochondrial activity, measured as mitochondrial membrane potential (MMP), into MMP^{high} and MMP^{low}. Whereas MMP^{low} HSCs are mostly quiescent, label-retaining, and with higher self-renewal, MMP^{high} HSCs are primed toward differentiation.[18,19]

Because metabolism tunes HSC fate, we wondered whether iron acts as an extrinsic regulator of HSC function by modulating their metabolic programs. To this aim, we studied 3 different mouse models of IO, including both mice treated with acute iron administration and animals affected by β-thalassemia (BThal) and sickle cell disease (SCD), which are inherited blood disorders characterized by chronic hemolytic anemia and IO.[20,21] In these diseases, previous studies from our group, and others, revealed impaired HSC self-renewal due to the prolonged residence into a damaged BM niche, with multiple stress signals.[22-29] However, the role of iron in contributing to HSC dysfunction has remained elusive.

Here, we showed that under IO conditions, most HSCs accumulate iron and ROS in mitochondria leading to low MMP and reduced OXPHOS despite high proliferation. We found that in the absence of functional mitochondria, active IO HSCs enhance glycolysis to sustain their energy requirement. Importantly, we proved that, in 2 models of anemia-associated chronic IO, in vivo reduction of iron and mitochondrial ROS (mtROS) restores normal HSC quiescence and function. Overall, our findings uncover that intracellular iron affects the metabolic programs underlying HSC function by controlling mitochondrial fitness through ROS generation.

Methods

Mouse models

Experiments were performed on adult, 12- to 14-week-old C57BL/6 and C57BL/6-CD45.1 (B/6.SJLCD45a-Pep3b) wild-type (WT) mice, and thalassemic C57BL6/$Hbb^{th3/+}$ mice (*th3*; The Jackson Laboratory; strain 002683), and humanized Townes SCD mice (*SS*) and SCD trait (*SA*) mice as controls (The Jackson Laboratory; strain 013071), bred in the laboratories at San Raffaele Hospital. Experimental and control mice were age- and sex-matched littermates for individual experiments.

In vivo treatments

To generate acute IO mouse model, female WT mice were treated with a single subcutaneous injection of iron dextran, 5 mg per mouse (Sigma).[30] To decrease mtROS in vivo, *th3* female mice were treated with 2 mg/kg mitochondria-specific antioxidant Mitoquinol (MitoQ, Cayman) through intraperitoneal injection for 5 days, as previously described.[31] For iron chelation experiments, *th3* and *SS* mice were injected daily for 14 days with deferoxamine (DFO; Sigma) 50 mg/kg, through intraperitoneal injection.[10]

Intracellular and mitochondrial iron content

To detect intracellular iron, lineage negative (Lin^-) cells were stained with 0.125μM calcein-acetoxymethyl ester (Invitrogen) for 5 minutes at 37°C. Then, cells were washed and stained for surface markers. To measure mitochondrial iron content, Lin^- cells were stained with 5μM Mito-FerroGreen (Dojindo) for 30 minutes at 37°C, after surface marker staining.

HSC transplantation

Competitive HSC transplantation assays were performed by transplanting 500 sorted HSCs (CD45.2) from *th3*, *th3* + MitoQ, *th3* + DFO, and WT donor mice, and 2 × 10^5 WT total BM supportive cells (CD45.1) into lethally irradiated (9 Gy in 2 split doses) WT recipients (CD45.1) by IV injection. Percentage of donor-derived cells in the peripheral blood (PB) of chimeric mice was determined by fluorescence-activated cell sorting at 4, 8, 12, and 16 weeks after transplantation. At termination (16 weeks), total BM cells were analyzed and injected into lethally irradiated WT secondary (CD45.1) recipients (dose of 1 × 10^6 cells per mouse), which were followed up to 16 weeks for PB chimerism. Chimeric mice were analyzed at termination (16 weeks) for BM chimerism, HSC cell cycle, and MMP analysis.

Statistical analyses

Data were analyzed by using GraphPad Prism version 8.0 software (La Jolla, CA). All data are presented as single values and mean ± standard error of the mean. The Mann-Whitney test was used for comparisons between 2 independent groups, and the Wilcoxon test for comparison between dependent groups. The Kruskal-Wallis test was performed for comparison among >2 independent groups, and Bonferroni correction was applied.

Further details on mouse models and experimental procedures have been included in the supplemental Materials and Methods, available on the *Blood* website.

All animal experiments were performed in accordance with approved protocols of the institutional animal care and use committees of San Raffaele Institute.

Results

IO induces mitochondrial dysfunction in HSCs

To explore the effects of iron accumulation in HSCs, we exploited the murine model of BThal (*th3*), one of the most common monogenic disorders worldwide characterized by chronic IO.[21] We previously demonstrated an impaired function of HSCs due to their persistence into an altered BM niche in *th3* mice.[24]

To assess whether iron is directly involved in HSC dysfunction, we first investigated any iron-related deregulation in their molecular profile by RNA sequencing of *th3* and WT HSCs,[24] phenotypically defined as SLAM HSCs (Lin^-, $cKit^+$, $Sca1^+$ $CD150^+$ $CD48^-$) cells[32,33] (supplemental Figure 1A). Interestingly, the 2 top-ranked Gene Ontology biological process categories enriched in *th3* HSCs were "transition metal ion homeostasis" and "iron ion homeostasis," followed by Gene Ontology categories associated with iron-heme homeostasis (Figure 1A). Consistently, analysis of differentially expressed genes showed a statistically significant upregulation of genes involved in iron transport and heme metabolism in *th3* HSCs, including ferritin (*Fth1*, *Ftl1*) and ferroportin (*Slc40a1*; Figure 1B; supplemental Table 1). Notably, *th3* HSCs showed a lower median

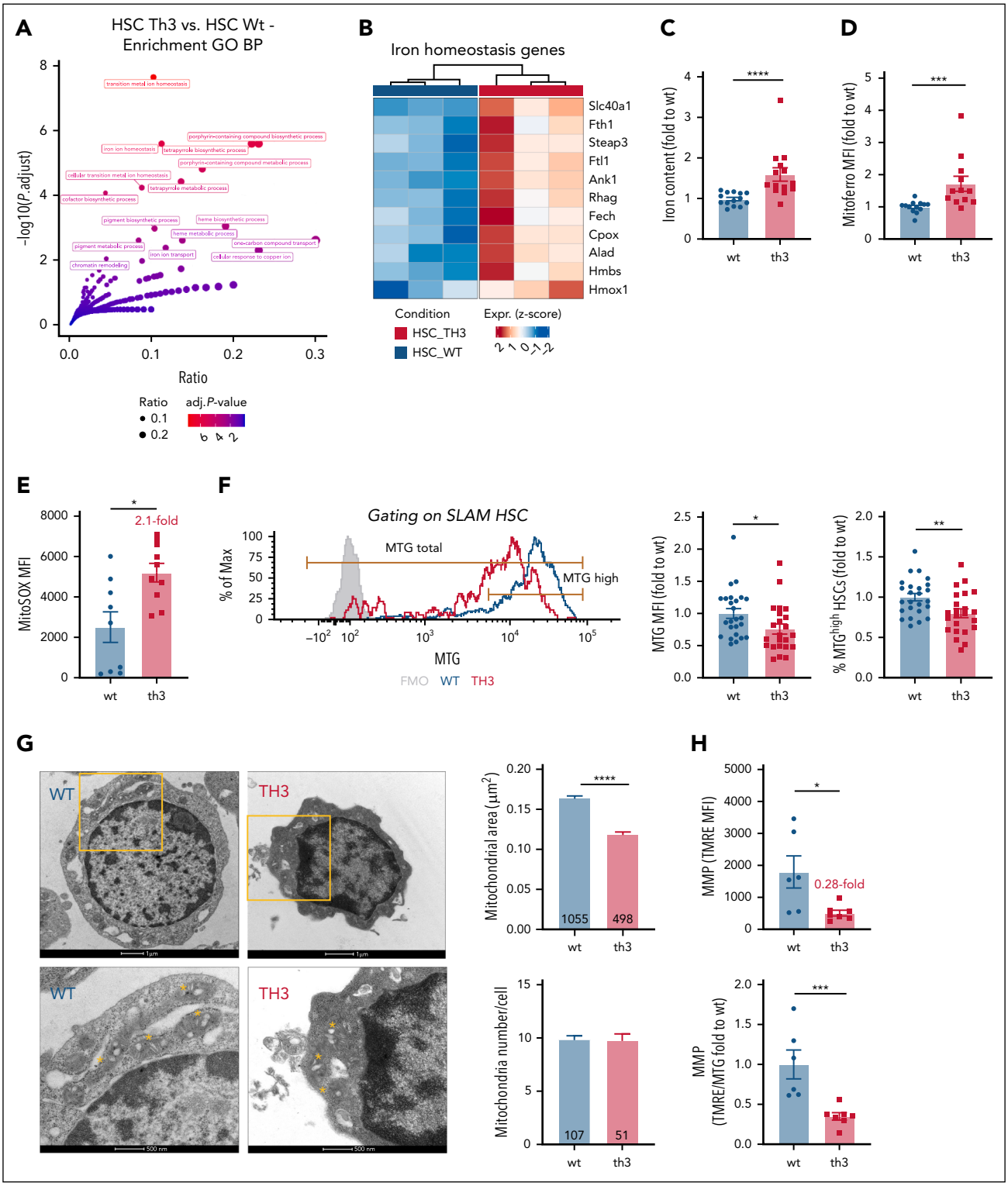

Figure 1. IO induces mitochondrial dysfunction in HSCs. (A) Enrichment plot of GO BP categories between *th3* and WT HSCs (n = 3). (B) Heat map of iron genes among differentially expressed genes (DEGs) between *th3* and WT HSCs (n = 3); false discovery rate of <0.1. (C) Intracellular iron content in WT and *th3* HSCs. Data were calculated as 1/MFI of calcein-acetoxymethyl ester (calcein-AM) and reported as fold to WT (n = 14). (D) Mitochondrial iron content in WT and *th3* HSCs. MFI of Mito-FerroGreen dye is expressed relative to WT (WT, n = 13; th3, n = 12). (E) mtROS in WT and *th3* HSCs. MFI of MitoSOX is reported (WT, n = 9; *th3*, n = 10). (F) Mitochondrial mass in WT and *th3* HSCs. Representative flow cytometry histogram (left), MFI of MTG (center) and percentage of MTG^{high} HSC (right) are reported. Data are expressed relative to WT (WT, n = 25; *th3*, n = 23). (G) Representative electron micrographs of WT and *th3* HSCs, a magnified view of the cell area highlighted in yellow is shown on the bottom. Yellow asterisks indicate mitochondria. Scale bar, 500 nm (left); quantification of size and number of mitochondria in WT and *th3* HSCs (right); "n" inside the bars indicates mitochondria numbers and cell numbers, respectively. (H) MMP in WT and *th3* HSCs. MFI of TMRE (upper) and TMRE:MTG ratio in HSCs (bottom) are reported. (WT, n = 6; *th3*, n = 7). If not specified otherwise, data are presented as mean ± standard error of the mean (SEM). Significance indicated as ****$P < .0001$; ***$P < .001$; **$P < .01$; *$P < .05$ was calculated using the Mann-Whitney test. BP, biological process; FMO, fluorescence minus one; GO, gene ontology; Max, maximum.

fluorescent intensity (MFI) of calcein-acetoxymethyl ester, an iron sensor whose fluorescence is quenched on binding to labile iron in the cytoplasm,[34,35] suggesting increased intracellular iron (Figure 1C; supplemental Figure 1B).

Given that mitochondria are the major hubs for iron storage and use, we labeled the mitochondrial iron pool with mito-FerroGreen and we found increased Fe^{2+} content, as free reactive iron, in *th3* HSCs (Figure 1D). No sex-specific differences were observed in iron content (supplemental Figure 1C-D). Consistent with the prooxidant activity of iron Fe^{2+}, *th3* HSCs accumulated 2.1-fold higher mtROS, detectable as increased MitoSOX MFI, which measures superoxide (Figure 1E).

To investigate the impact of iron excess in the mitochondria of HSCs, we analyzed mitochondrial properties in BThal. Labeling with Mitotracker Green (MTG) revealed a lower total MFI in *th3* HSCs and a reduced frequency of MTG^{high} HSCs, thus indicating reduced mitochondrial mass (Figure 1F). Transmission electron microscopy analyses on sorted HSCs confirmed the reduced size of mitochondria, whereas no differences were found in the number of mitochondria per cell (Figure 1G). Consistently, we found reduced expression of the major regulators of mitochondrial biogenesis, *Tfam* and *Tfb1m* and of key players of mitophagy, such as *Gabarapl1* and *Map1lc3b* (supplemental Figure 2A-B).

To assess whether the defective mitochondria were still functional, we measured MMP by the cationic fluorescent probe tetramethylrhodamine ethyl ester (TMRE) and we found a lower MMP in *th3* HSCs, indicating reduced mitochondrial activity, regardless of their decreased mass (Figure 1H).

Collectively, these data reveal that the HSC compartment accumulates free reactive iron in mitochondria in IO condition and that HSCs with IO show mitochondrial perturbations.

Active IO HSCs proliferate despite reduced mitochondrial function

The analysis of HSC based on TMRE intensity, as previously reported,[18,19,31] showed a reduced fraction of MMP^{high} and a higher proportion of MMP^{low} HSCs in *th3* mice (Figure 2A). Given the lower number of *th3* HSCs (Figure 2B, left), the absolute counts of both MMP^{low} and MMP^{high} HSCs were lower in *th3* mice than in WT mice (Figure 2B, right), with an 80% reduction in MPP^{high} HSCs, indicating a predominant reduction in this fraction. Because MMP^{high} HSCs were reported to be actively proliferating,[18] we explored whether IO HSCs could proliferate in the presence of damaged mitochondria. Cell cycle analysis revealed an increased proportion of active *th3* HSCs (Figure 2C), with a higher fraction of cells in G1 phase at the expense of the quiescent G0 phase (Figure 2D). We coupled the analysis of mitochondrial function and HSC cell cycle by performing single-cell division assay of sorted MMP^{low} *th3* and WT HSCs (Figure 2E; supplemental Table 2). After 48 hours of in vitro single-cell culture, 20% of *th3* MMP^{low} HSCs did not divide compared with 34% of WT cells (Figure 2F, left). Furthermore, *th3* MMP^{low} HSCs undergoing >2 cell divisions were threefold more abundant than WT, thus indicating a cycling-primed state (Figure 2F, right). These data demonstrate that *th3* HSCs divide more frequently despite the lower mitochondrial activity.

IO HSCs have reduced OXPHOS and rely on glycolysis for energy production

To determine whether the reduced MMP of IO HSCs resulted in impaired mitochondrial OXPHOS metabolism, we performed the Seahorse metabolic flux analysis of Lin^- hematopoietic progenitor cells. *th3* cells showed increased proton leak, indicating a higher proportion of basal respiration uncoupled from ATP production, and an eightfold reduction in spare respiratory capacity, likely reflecting reduced mitochondrial capacity to produce additional energy under stress (Figure 3A). To confirm these findings also in the primitive HSC compartment, we measured ATP in sorted *th3* HSCs with or without oligomycin, which blocks the activity of mitochondrial ATP synthase (Figure 3B). Total ATP in *th3* HSCs was half of that in WT controls. Lower ATP content in *th3* HSCs could result from reduced overall ATP production or increased ATP consumption. Notably, inhibition of OXPHOS by oligomycin resulted in 50% reduction of ATP in WT cells but only 24% reduction in *th3* HSCs (Figure 3C), thus indicating that IO HSCs have reduced OXPHOS-dependent energy production. Because glycolysis is the only metabolic pathway able to generate ATP when mitochondria do not function, we conclude that the ATP produced after oligomycin treatment derives from glycolysis.

To test our hypothesis of glycolysis dependency, we measured glucose uptake, and higher fluorescence of the glucose analogue 2-[*N*-(7-nitrobenz-2-oxa-1,3-diazol-4-yl)amino]-2-deoxy-D-glucose (2NBDG) in *th3* HSCs indicated increased glycolytic flux (Figure 3D). Consistently, our RNA-sequencing data on sorted *th3* HSCs showed upregulated expression of the glycolytic enzymes *Tpi1*, *Minpp1*, *Gapdh*, and *Pklr* (Figure 3E). These data suggest the possibility that IO HSCs potentiate glycolysis to compensate for reduced OXPHOS. Untargeted metabolomics on sorted primitive hematopoietic stem progenitor cells (HSPCs), phenotypically defined as $Lin^-cKit^+Sca1^+$ revealed substantial changes in metabolite content (supplemental Figure 3A), with significant difference between *th3* and WT samples in glycolysis/gluconeogenesis, fructose and mannose metabolism, and pyruvate metabolism (Figure 3F; supplemental Table 3). Notably, glycolysis/gluconeogenesis was the most differentially enriched metabolic pathway. IO HSPCs exhibited a high content of the glycolytic intermediates α-D-glucose 6-phosphate, 2-phospho-D-glycerate, and 3-phospho-D-glycerate (Figure 3G), which matched with increased expression of glycolytic genes (Figure 3E). Intracellular lactate was reduced (Figure 3H), possibly resulting from consumption or extrusion in the extracellular space.[36] In line with reduced OXPHOS, we found that several tricarboxylic acid (TCA) cycle–related metabolites were downregulated in *th3* samples, such as citrate, succinate, fumarate, and malate (supplemental Figure 3B), and correlated with the expression of their corresponding enzymes (supplemental Figure 3C).

Taken together, our data disclosed an overall rewiring of cellular metabolism in IO BThal HSCs, with increased glycolytic dependency to compensate for reduced OXPHOS caused by mitochondrial dysfunction.

Intracellular iron controls HSC metabolism

To validate our proof of concept in a model of IO different from the disease context of BThal and to demonstrate the specific

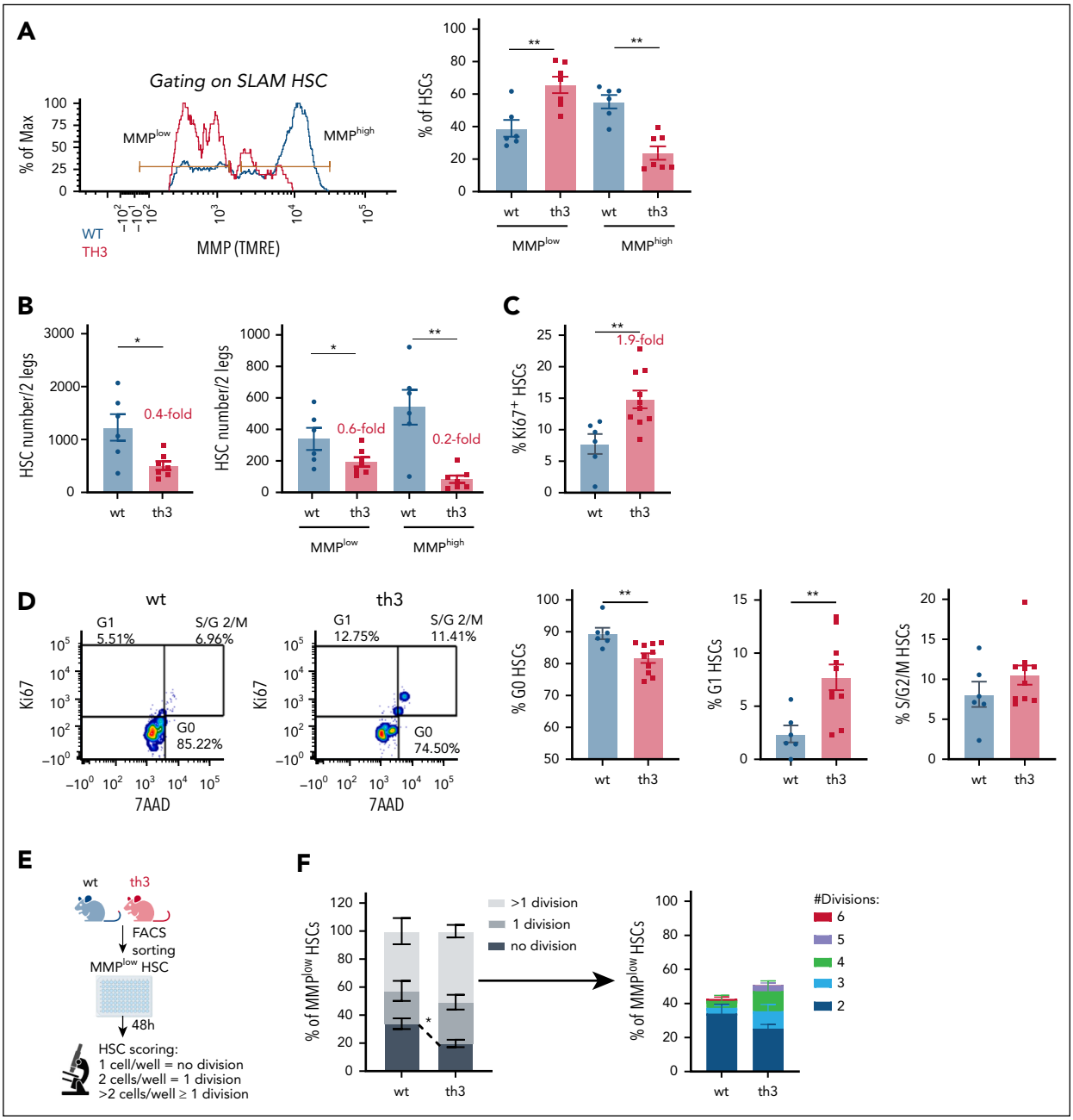

Figure 2. Active IO HSCs proliferate despite low mitochondrial function. (A) Classification of WT and *th3* SLAM HSCs based on TMRE MFI as MMP^{high} and MMP^{low} HSCs. Representative flow cytometry histogram and percentage of cells is reported (WT, n = 6; th3, n = 7). (B) Total number of HSCs (left) and MMP^{high}, MMP^{low} HSCs (right) in the BM of WT and *th3* mice (WT, n = 6; *th3*, n = 7). (C) Percentage of proliferating HSCs (Ki67^{+}) in WT and *th3* mice (WT, n = 6; *th3*, n = 10). (D) Evaluation of cell cycle distribution among G0, G1, and S/G2/M phases of WT and *th3* HSCs after 7-AAD/Ki-67 staining. Representative FACS plot (left) and quantification (right) are reported (WT, n = 6; *th3*, n = 10). (E) Scheme of single-cell division assay in sorted MMP^{low} HSCs. (F) Single-cell division assay after 48 hours in WT and *th3* MMP^{low} HSCs. The percentage of cells is shown (WT, n = 4; *th3*, n = 3). If not specified otherwise, data are presented as mean ± SEM. Significance indicated as $^{**}P < .01$; $^{*}P < .05$ was calculated using Mann-Whitney test. 7-AAD, 7-amino-actinomycin D; FACS, fluorescence-activated cell sorting.

role of IO on HSC metabolism, we treated WT mice with iron dextran[30] (Figure 4A). The generated IO mouse model (WT_IO) displayed intracellular IO (Figure 4B; supplemental Figure 4A) and higher accumulation of mtROS (Figure 4C).

We examined the morphology of mitochondrial network by 3-dimensional immunofluorescence analyses of the amount and distribution of mitochondrial-specific protein translocase of outer membrane 20 (TOM20) in sorted WT_IO HSCs. Despite comparable total fluorescent intensity of TOM20 (supplemental Figure 4B), the mitochondria of WT_IO HSCs were more fragmented (Figure 4D), as assessed by the higher number and lower volume per cell of mitochondria labeled by TOM20 (Figure 4E-F), suggesting increased mitochondrial fission. Dynamin-related protein 1 (DRP1), the main mitochondrial fission regulator, oligomerizes onto mitochondria membrane to initiate mitochondrial division.[37] Notably, we detected an increased number of DRP1 fragments (supplemental Figure 4C) and enhanced DRP1

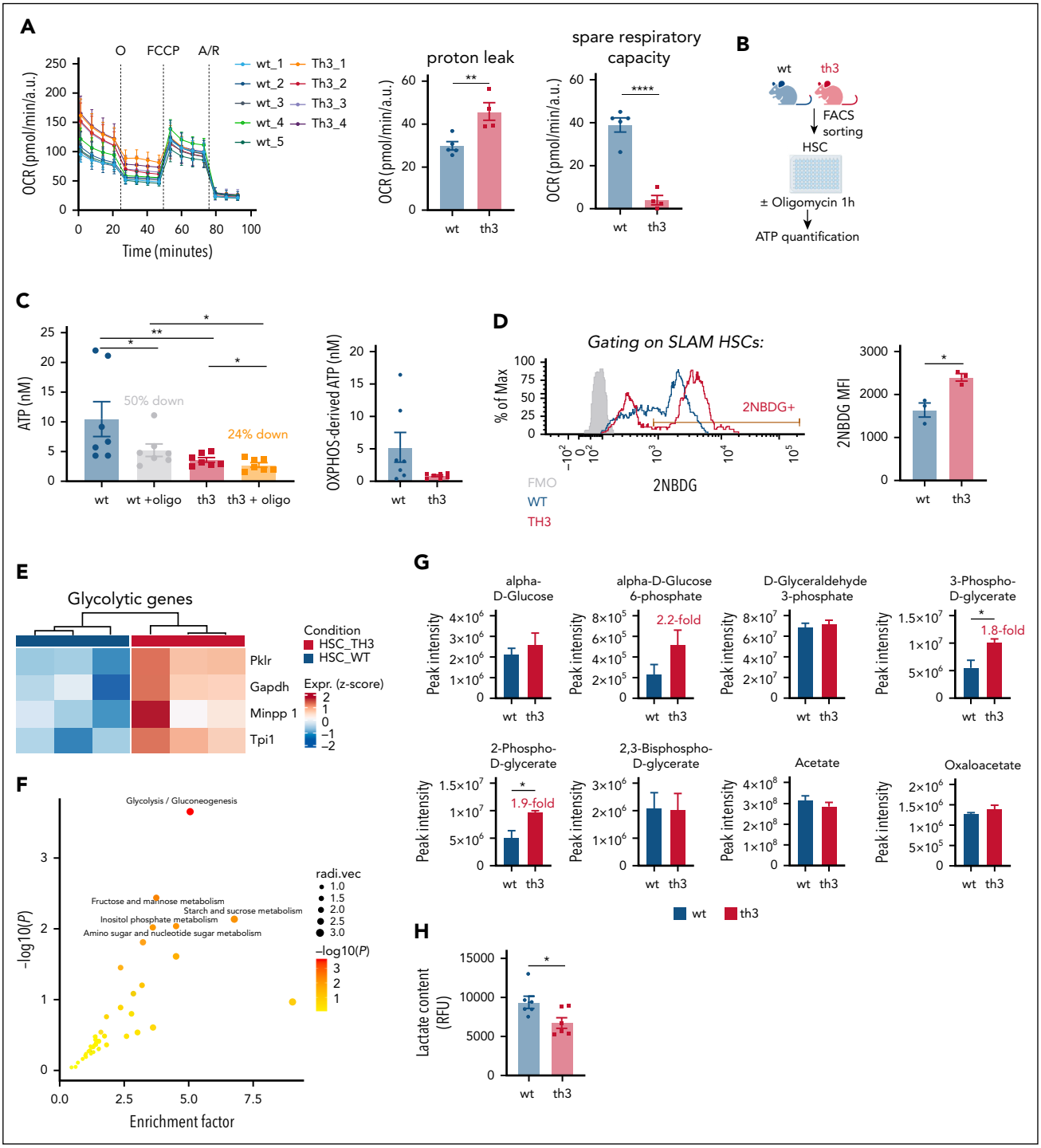

Figure 3. IO HSCs have reduced OXPHOS and rely on glycolysis for energy production. (A) Mitochondrial respiration measured as OCR in *th3* and WT Lin$^-$ cells. OCR profiles (left) and quantification of proton leak and spare respiratory capacity (right) (WT, n = 5; *th3*, n = 4). (B) Scheme of measuring ATP content with or without oligomycin in sorted WT and *th3* HSCs. (C) ATP content with or without oligomycin treatment (left) and quantification of OXPHOS-derived ATP (right) in 500 sorted WT and *th3* HSCs (n = 7). Data are presented as mean ± SEM. Significance indicated as $^{**}P < .01$; $^{*}P < .05$ was calculated using Mann-Whitney test for WT vs *th3* and for WT + oligo vs *th3* + oligo and Wilcoxon test for untreated vs treated samples. (D) Glucose uptake in WT and *th3* HSCs. Representative flow cytometry histogram (left) and MFI in 2NBDG$^+$ HSC (right) are reported (n = 3). (E) Heat map of glycolytic genes among DEGs between *th3* and WT HSCs (n = 3). (F) Heat map showing metabolic pathways that significantly differ between *th3* and WT HSPCs with Mummichog pathway analysis (n = 4). (G) Quantification (peak intensity) of glycolytic metabolites in glycolysis/gluconeogenesis pathway in WT and *th3* HSPCs (n = 4). Data are presented as mean ± SEM. Significance indicated as $^{*}P < .05$ was calculated using unpaired *t* test. (H) Lactate content in 500 sorted WT and *th3* HSCs (n = 6). If not specified otherwise, data are presented as mean ± SEM. Significance indicated as $^{****}P < .0001$; $^{*}P < .05$ was calculated using Mann-Whitney test. A/R, antimycin/rotenone; FACS, fluorescence-activated cell sorting; FCCP, carbonyl cyanide-4 (trifluoromethoxy) phenylhydrazone; FMO, fluorescence minus one; Gapdh, glyceraldehyde-3-phosphate dehydrogenase; Minpp1, multiple inositol polyphosphate phosphatase 1; O, oligomycin; OCR, oxygen consumption rates; oligo, oligomycin; Pklr, pyruvate kinase; RFU, relative fluorescence unit; Tpi1, triosephosphate isomerase 1.

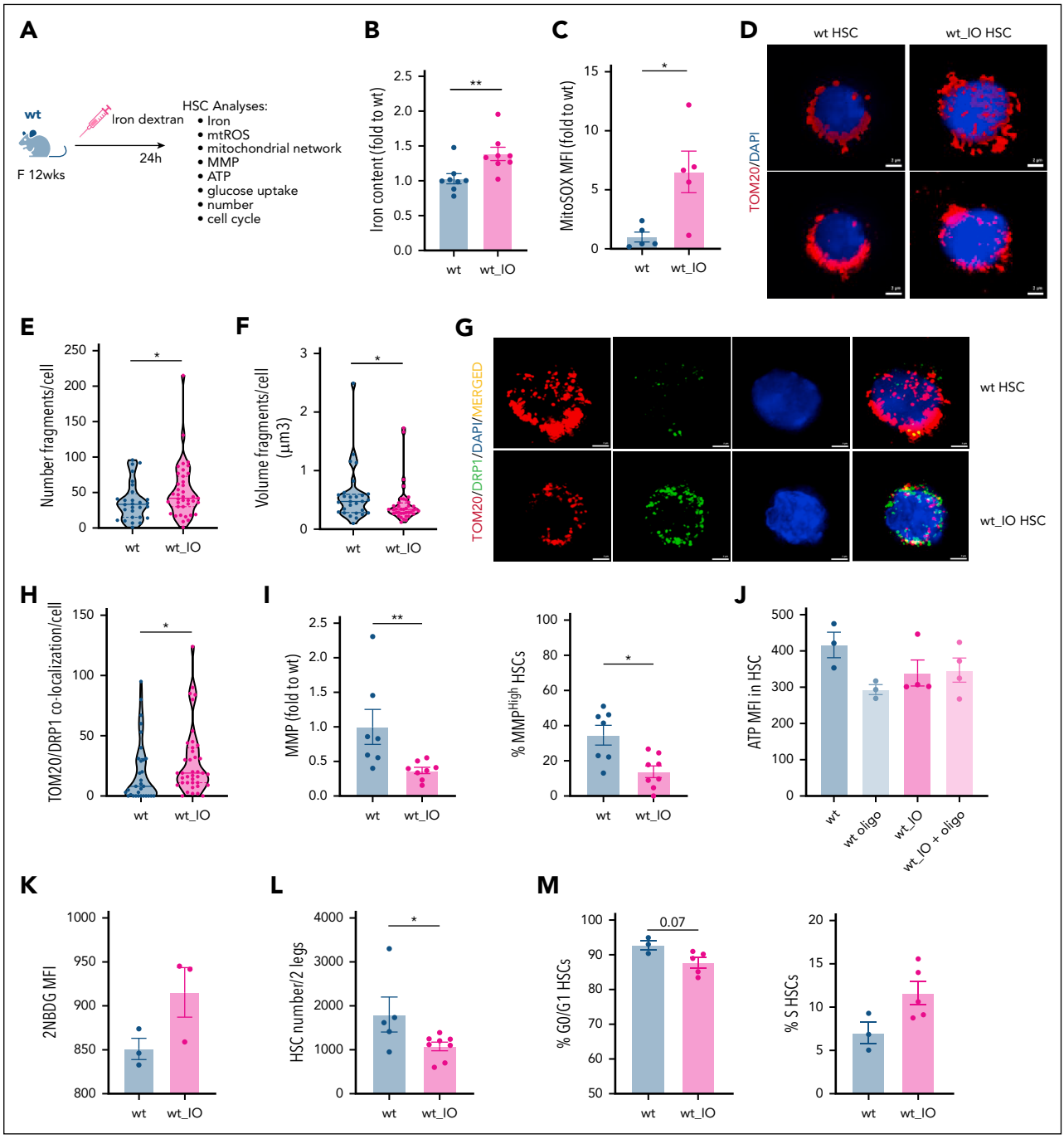

Figure 4. Intracellular iron controls HSC metabolism. (A) Scheme of generation of IO mouse model and analyses performed on WT_IO HSCs. (B) Intracellular iron content in WT and WT_IO HSCs. Data were calculated as 1/MFI of calcein-AM and reported as fold to WT (n = 8). (C) mtROS in WT and WT_IO HSCs. MFI of MitoSOX is reported. Data are expressed relative to WT (n = 5). (D) Representative 3-dimensional (3D) immunofluorescent images of TOM20 in WT and WT_IO HSC (red, TOM20; blue, DAPI [4′,6-diamidino-2-phenylindole]; scale bar, 2 µm). (E) Total number of mitochondrial (TOM20) fragments per HSC (WT, n = 39 cells, WT_IO, n = 31 cells). (F) Average volume of mitochondrial TOM20 fragments per HSC (WT, n = 39 cells, WT_IO, n = 31 cells). (G) Representative 3D immunofluorescent images of TOM20 (red), DRP1 (green), DAPI (blue), merged (yellow) in WT and WT_IO HSC (scale bar, 2 µm). (H) Quantification of colocalization of TOM20 and DRP1 in WT and WT_IO HSCs (WT, n = 39 cells, WT_IO, n = 31 cells). (I) MMP in WT and WT_IO HSCs. MFI of TMRE (left) and percentage of MMP^{high} HSCs (right) (WT, n = 7; WT_IO, n = 8). (J) ATP content with or without oligomycin treatment in WT and WT_IO HSCs. MFI of ATP is reported (WT, n = 3; WT_IO, n = 4). (K) Glucose uptake in WT and WT_IO HSCs. MFI in $2NBDG^{+}$ HSC is reported (n = 3). (L) Total number of HSCs in the BM of WT and WT_IO mice (WT, n = 5; *th3*, n = 8). (M) Percentage of quiescent (G0/G1 phase) and cycling (S phase) HSCs in WT and WT_IO mice (WT, n = 3; and WT_IO, n = 5). If not specified otherwise, data are presented as mean ± SEM. Significance indicated as $^{**}P < .01$; $^{*}P < .05$ was calculated using Mann-Whitney test. F, female.

localization to mitochondria (Figure 4G-H) in WT_IO HSCs, thus demonstrating that iron reshapes the mitochondrial network by promoting mitochondrial fission. Consistently, also *th3* HSCs showed increased mitochondrial fission (supplemental Figure 4D-E). Mitochondrial fission typically generates smaller mitochondria with low MMP[38] and the reduced MMP of WT_IO

HSCs (Figure 4I; supplemental Figure 4F) suggests that increased DRP1-mediated mitochondrial fragmentation may contribute to impaired mitochondrial activity of IO HSCs or may be a compensatory mechanism to prevent HSC proliferation and exhaustion.

Strikingly, we found that higher iron content corresponds to lower mitochondrial activity in HSCs, as shown by the positive correlation between TMRE and calcein levels (supplemental Figure 4G). Wt_IO HSCs had reduced ATP and, upon OXPHOS inhibition by oligomycin treatment, did not show a change in ATP as compared with controls (Figure 4J). Moreover, WT_IO HSCs showed increased glucose uptake, as assessed by higher fluorescence of the glucose analogue 2NBDG (Figure 4K), mirroring the status of HSCs with low OXPHOS and increased glycolysis dependency in BThal (see Figure 3). IO mice exhibited a reduced number of HSCs (Figure 4L), which was comparable with that of IO *th3* mice (supplemental Figure 4H) and IO HSCs were more proliferating, with a lower frequency of cells in G0/G1 phase and an increased proportion of cells in S phase (Figure 4M), suggesting that IO triggers HSC exhaustion by inducing their cell cycle entry and proliferation.

Collectively, this set of data clearly reveals that intracellular IO promotes mitochondrial fragmentation, reduces mitochondrial activity, and drives metabolic adaptations in HSCs.

Iron chelation restores mitochondrial dysfunction of IO HSCs

As definitive proof of the role of iron on HSC mitochondrial defect and metabolism, we reduced intracellular iron in *th3* mice. We injected *th3* mice for 14 days with the iron chelator, DFO (Figure 5A). DFO treatment was not able to rescue BThal ineffective erythropoiesis or anemia (supplemental Figure 5A-B), in line with a previous report.[10] This regimen efficiently normalized intracellular and mitochondrial iron content (Figure 5B; supplemental Figure 5C-D) and mtROS in HSCs (Figure 5C; supplemental Figure 5E), rescued mitochondrial dysfunction (Figure 5D; supplemental Figure 5F), enhanced ATP (Figure 5E; supplemental Figure 5G), and reduced glucose uptake in *th3* HSCs (Figure 5F; supplemental Figure 5H). Upon DFO administration we found restored HSC frequency and number along with an increased frequency of HSCs in G0/G1 phase, and a proportion of HSCs in S phase reduced to WT levels (Figure 5G-H; supplemental Figure 5I-J).

We next assessed whether IO may contribute to the functional decline of BThal HSCs[24,25] (supplemental Figure 6A-B) by performing serial HSC transplantation experiments. We proved that DFO treatment significantly improved the self-renewal of long-term repopulating *th3* HSCs (Figure 5I), by rechallenging HSC function in a serial transplantation setting (supplemental Figure 6C). Limited difference in donor engraftment between *th3* + DFO and *th3* cells in primary transplant (supplemental Figure 6D) supports the evidence of functional rescue at the level of long-term repopulating compartment.

These results demonstrate that IO impairs HSC mitochondrial activity and metabolism, and negatively affects their size, quiescence, and self-renewal in BThal.

IO-derived oxidative stress impairs HSC function by causing mitochondrial dysfunction

The complete normalization of mtROS content after DFO administration indicated that IO is the primary cause of oxidative stress in *th3* HSCs. To confirm that elevated mtROS mediate iron toxicity on mitochondria, we targeted them in vivo by injecting BThal mice with MitoQ for 5 days (Figure 6A). In contrast to DFO treatment (see supplemental Figure 5B) MitoQ increased hemoglobin levels and red blood cell count (supplemental Figure 7A). MitoQ treatment efficiently reduced mtROS levels (supplemental Figure 7B), without affecting iron content (supplemental Figure 7C), and enhanced mitochondrial activity in *th3* HSCs (Figure 6B; supplemental Figure 7D), thus indicating that oxidative stress is the cause of mitochondrial dysfunction. Next, we tested HSC glycolytic metabolism in treated *th3* mice and we found it restored to normal levels (Figure 6C; supplemental Figure 7E), similarly to the effect of iron chelation (see Figure 5F).

Intracellular IO and oxidative stress were reported to be deleterious for HSC function.[10,11,13,39] We next assessed whether IO-derived mtROS may contribute to the functional decline of BThal HSCs.[24,25] We first investigated the HSC frequency and cell cycle after MitoQ administration. MitoQ treatment restored to normal the frequency of *th3* HSCs (Figure 6D) and the proportion of HSCs in quiescent G0/G1 phase of cell cycle (Figure 6E). To study the repopulating ability and self-renewal of long-term HSCs, we performed serial HSC transplantation experiments (Figure 6F). Upon HSC rechallenge by secondary transplantation, *th3* + MitoQ HSCs provided higher donor engraftment in the PB, total BM, and HSC compartment (Figure 6G-H), and enhanced quiescence (Figure 6I) than in untreated *th3* HSCs. Importantly, reduction of IO-derived mtROS reconstituted an HSC pool with enhanced mitochondrial activity compared with that derived from *th3* untreated donors (Figure 6J). Limited differences in donor engraftment between *th3* + MitoQ and *th3* cells upon primary transplantation confirmed that MitoQ treatment specifically targets the long-term repopulating ability of HSCs (supplemental Figure 7F-G).

Overall, our results demonstrate that excessive IO-derived mtROS alter BThal HSC quiescence and self-renewal by impairing mitochondrial activity and cellular metabolism.

IO induces mitochondrial alterations also in SCD

To assess whether a similar mitochondrial rewiring is present in other hematopoietic disorders with chronic IO, we exploited the murine model of SCD, the *SS* mice.[20,40] *SS* mice have reduced HSC number with high ROS and DNA damage due to impaired supportive capacity of the stromal niche.[27]

Similarly to what was observed in WT_IO and BThal HSCs, we detected intracellular and mitochondrial IO in *SS* HSCs as compared with asymptomatic controls (Figure 7A-B), with oxidative stress in the mitochondria (Figure 7C). Investigating HSC metabolism, we found reduced total ATP production (Figure 7D) with an increased glucose uptake (Figure 7E), indicating a metabolic shift toward glycolysis. Also, in *SS* mice, MMP was lower, with a reduced frequency of MMP^{high} HSCs, which was restored by DFO treatment (Figure 7F-G), demonstrating that intracellular IO causes mitochondrial dysfunction and subsequent metabolic adaptations of HSCs in SCD.

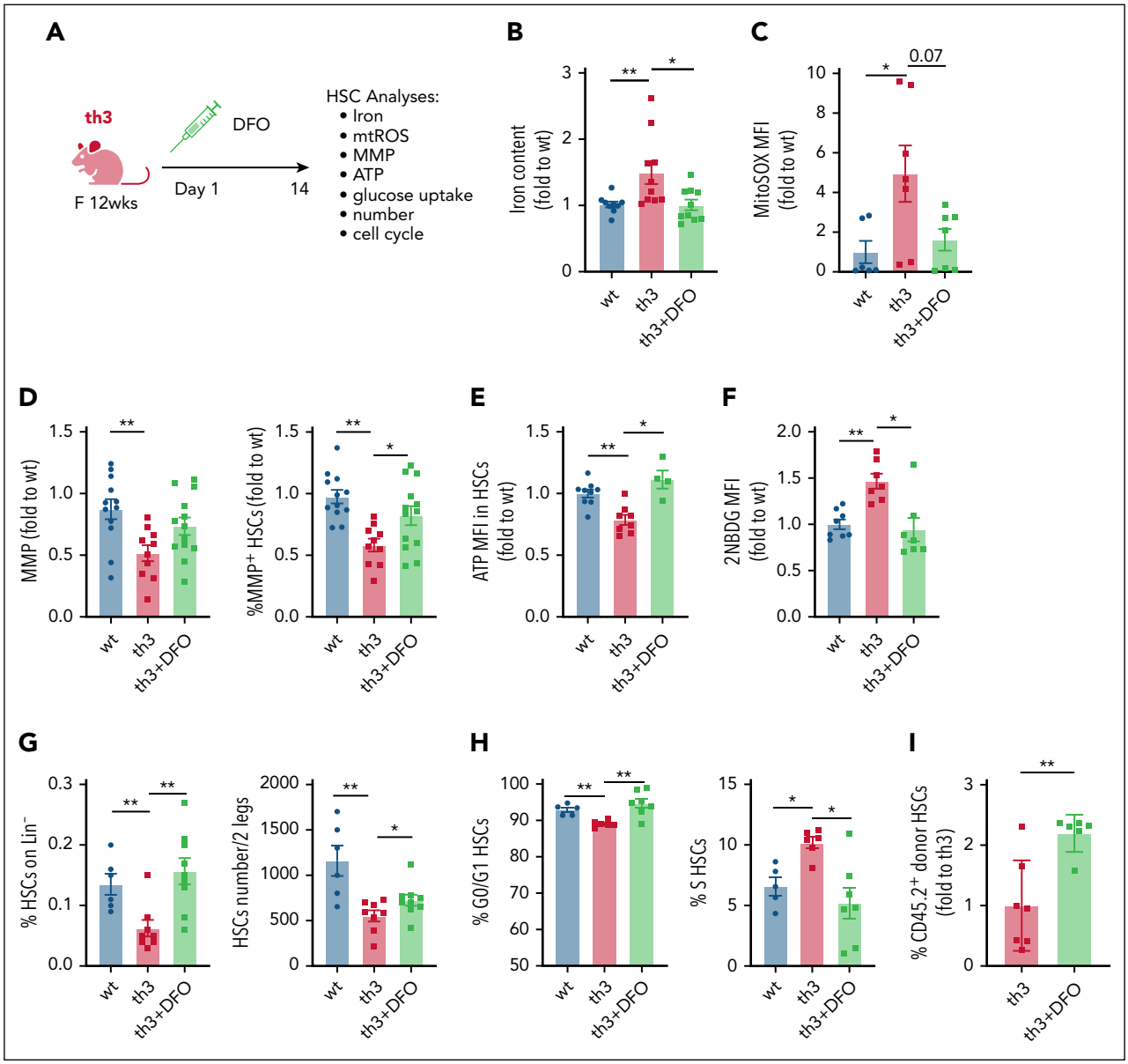

Figure 5. Iron chelation restores mitochondrial dysfunction of IO HSCs. (A) Scheme showing iron chelation regimen of *th3* mice by DFO and analyses performed on HSCs. (B) Intracellular iron content in WT, *th3*, and *th3* + DFO HSCs. Data were calculated as 1/MFI of calcein-AM and reported as fold to WT (WT, n = 9; *th3*, n = 10; *th3* + DFO, n = 10). (C) mtROS in WT, *th3*, and *th3* + DFO HSCs. MFI of MitoSOX is reported. Data are expressed relative to WT (WT, n = 6; *th3*, n = 7; *th3* + DFO, n = 7). (D) MMP in WT, *th3*, and *th3* + DFO HSCs. MFI of TMRE (left), percentage of MMP^+ HSCs (right). Data are expressed relative to WT (WT, n = 12; *th3*, n = 10; *th3* + DFO, n = 13). (E) ATP content in WT, *th3*, and *th3* + DFO HSCs. MFI of ATP is reported. Data are expressed relative to WT (WT, n = 9; *th3*, n = 8; *th3* + DFO, n = 4). (F) Glucose uptake in WT, *th3*, and *th3* + DFO HSCs. MFI in $2NBDG^+$ HSC is reported. Data are expressed relative to WT (WT, n = 8; *th3*, n = 7; *th3* + DFO, n = 7). (G) Frequency and total number of WT, *th3*, and *th3* + DFO HSCs in the BM (WT, n = 6; *th3*, n = 8; *th3* + DFO = 9). (H) Percentage of quiescent (G0/G1 phase) and cycling (S phase) HSCs in WT, *th3*, and *th3* + DFO mice (WT, n = 5; *th3*, n = 6; *th3* + DFO = 7). (I) Chimerism of *th3* and *th3* + DFO HSCs at 16 weeks after secondary transplantation in lethally irradiated recipients (*th3*, n = 7; *th3* + DFO = 6). If not specified otherwise, data are presented as mean ± SEM. Significance indicated as $^{**}P < .01$; $^{*}P < .05$ was calculated using Kruskal-Wallis test. F, female.

Overall, these findings are indicative of an impaired network connecting iron to mitochondria in HSCs as a common feature of hematological disorders characterized by chronic IO.

Discussion

The maintenance of intracellular iron homeostasis is known to guarantee proper HSC self-renewal and differentiation. Iron restriction was found to promote fatty acid oxidation under regenerative stress.[10] Here, we unveiled that intracellular IO rewires the metabolic programs underlying HSC function. Exploiting BThal and SCD, as ideal models of chronic and robust IO, and providing iron to WT mice, we discovered 3 additional key findings: (1) intracellular IO impairs mitochondrial activity and OXPHOS of HSCs; (2) glycolysis sustains the metabolism of active HSCs in absence of functional mitochondria; and (3) the restoration of mitochondrial fitness after in vivo normalization of IO-derived mtROS rescues the quiescence and function of BThal HSCs. In sum, iron acts as extrinsic regulator of HSC metabolism and its targeting might represent a strategy to preserve HSC function in blood disorders with IO.

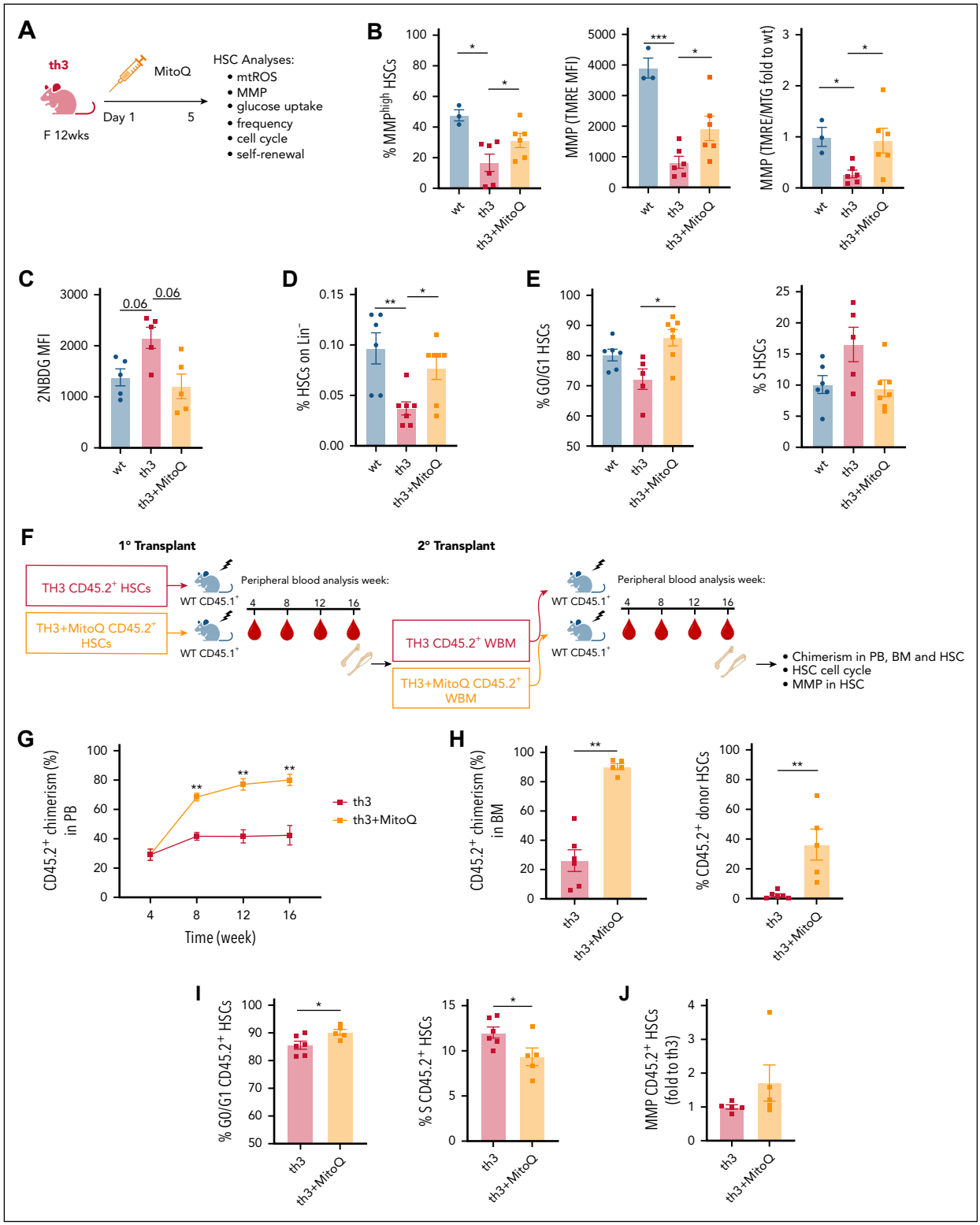

Figure 6. IO-derived oxidative stress impairs HSC function by causing mitochondrial dysfunction. (A) Scheme showing the reduction of mtROS in *th3* mice by MitoQ treatment and analyses performed on HSCs. (B) MMP in WT, *th3*, and *th3* + MitoQ HSCs. Percentage of MMP^{high} HSCs (left), MFI of TMRE (center), and TMRE/MTG ratio in HSCs (right) are reported (WT, n = 3; *th3*, n = 6; *th3* + MitoQ, n = 6). (C) Glucose uptake in WT, *th3*, and *th3* + MitoQ HSCs. MFI in 2NBDG$^+$ HSC is reported (n = 5). (D) Frequency of WT, *th3*, and *th3* + MitoQ HSCs on BM Lin$^-$ cells (WT, n = 6; *th3*, n = 7; *th3* + MitoQ = 7). (E) Percentage of quiescent HSCs (G0/G1 phase) and cycling (S phase) in WT, *th3*, and *th3* + MitoQ mice (WT, n = 6; *th3*, n = 5; *th3* + MitoQ = 7). (F) Scheme of serial transplantation of *th3* and *th3* + MitoQ HSCs and analyses performed. Primary transplant: 500 sorted HSCs (CD45.2) were transplanted with 2×10^5 WT total BM supportive cells (CD45.1) into lethally irradiated (9 Gy in 2 split doses) WT recipients (CD45.1). Secondary transplant: 1×10^6 cells total BM (WBM) cells from primary recipients were injected into lethally irradiated WT secondary recipients (CD45.1). (G) Engraftment of *th3* and *th3* + MitoQ HSCs in the PB at 4, 8, 12, and 16 weeks after secondary transplantation in lethally irradiated recipients (*th3*, n = 6; *th3* + MitoQ = 5). (H) Engraftment of *th3* and *th3* + MitoQ HSCs in the BM at 16 weeks after secondary transplantation in lethally irradiated recipients (left) and HSC chimerism (right) (*th3*, n = 6; *th3* + MitoQ = 5). (I) Percentage of quiescent (G0/G1 phase) and cycling (S phase) grafted HSCs (*th3*, n = 6; *th3* + MitoQ = 5). (J) MMP of grafted HSCs derived from *th3* and *th3* + MitoQ donors at 16 weeks after secondary transplantation in lethally irradiated recipients. MFI

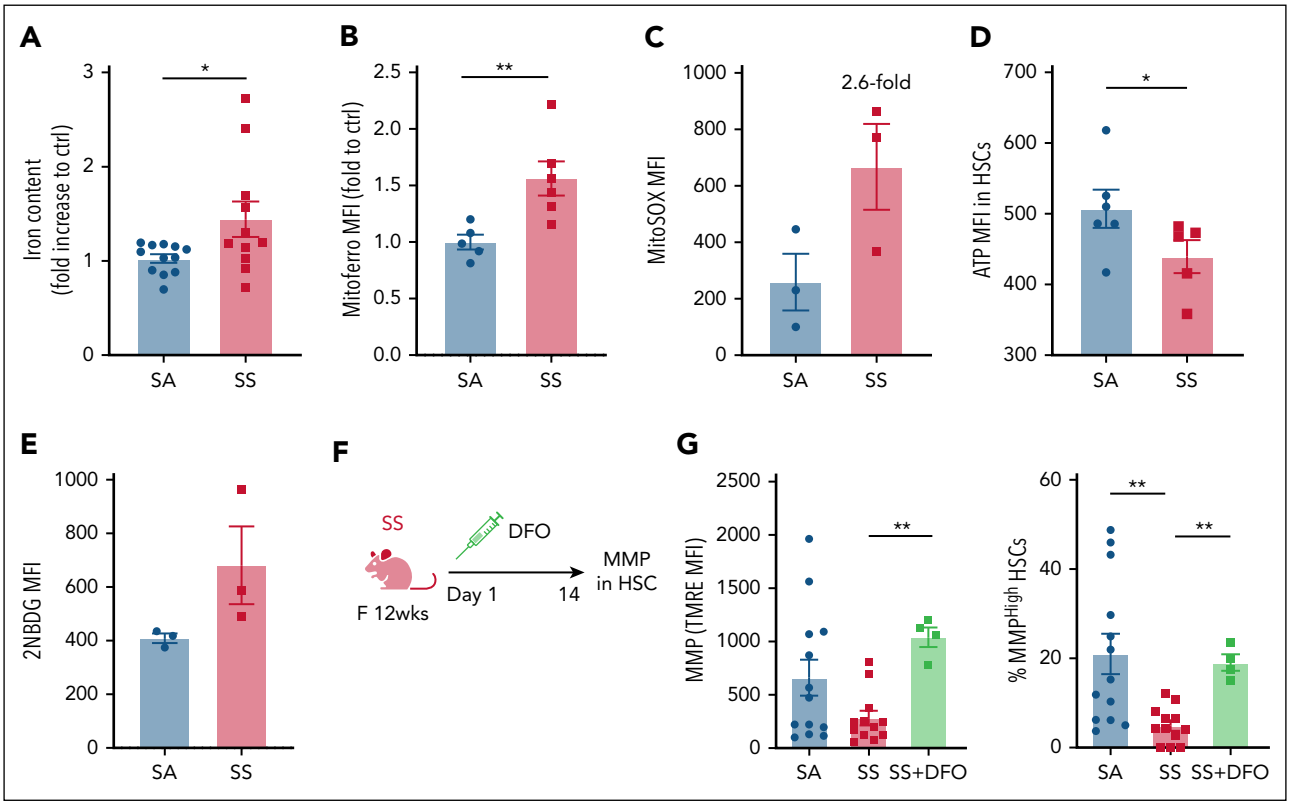

Figure 7. IO induces mitochondrial alterations also in SCD. (A) Intracellular iron content in *SA* and *SS* HSCs. Heterozygous *SA* sickle trait mice were used as controls in all our experiments because they do not harbor any disease-related abnormalities. Data were calculated as 1/MFI of calcein-AM and reported as fold to *SA* (*SA*, n = 12; *SS*, n = 11). (B) Mitochondrial iron content in *SA* and *SS* HSCs. MFI of Mito-FerroGreen dye is reported. Data are expressed relative to *SA* (*SA*, n = 5; *SS*, n = 6). (C) mtROS in *SA* and *SS* HSCs. MFI of MitoSOX is reported (n = 3). (D) ATP content in *SA* and *SS* HSCs. MFI in ATP$^+$ HSC is reported (*SA*, n = 6; *SS*, n = 5). (E) Glucose uptake in *SA* and *SS* HSCs. MFI in 2NBDG$^+$ HSC is reported (n = 3). (F) Scheme showing iron chelation regimen of *SS* mice by DFO and MMP analysis performed on HSCs. (G) MMP in *SA*, *SS*, and *SS* + DFO HSCs. MFI of TMRE (left) and percentage of MMP^{high} HSCs (right) are reported (*SA*, n = 13; *SS*, n = 12; *SS* + DFO, n = 4). If not specified otherwise, data are presented as mean ± SEM. Significance indicated as $^{**}P < .01$; $^{*}P < .05$ was calculated using Mann-Whitney test for panels A-E, or Kruskal-Wallis test for panel G. F, female.

In disorders with chronic IO, HSCs accumulated free reactive iron, high mtROS, small mitochondria with low MMP, and reduced OXPHOS. In WT mice, a single dose of iron was sufficient to generate mtROS, reduce mitochondrial activity, impair OXPHOS, and decrease ATP in HSCs.

Changes in HSC cell cycle and functional state determine metabolic adaptations and, vice versa, metabolism controls HSC cell cycle and function,[16] raising the unsolved question about what comes first. Although we cannot exclude that mtROS arise from different processes in the cell, the normalization of mtROS content after DFO administration indicated that IO is the main cause of mitochondrial oxidative stress in BThal HSCs. In vivo reduction of IO-derived mtROS in BThal mice restored HSC frequency, quiescence, and function, and, more importantly, the improved HSC self-renewal was accompanied by a restored mitochondrial activity upon transplantation. Based on this, we propose that excess of intracellular iron and mtROS act upstream of the mitochondrial function and metabolism, thus modulating HSC function.

Fission events generate depolarized mitochondria with low MMP, which are removed through mitophagy.[38] Enhanced mitochondrial fragmentation via DRP1 in BThal and WT_IO HSCs indicates that mitochondrial fission contributes to impaired mitochondrial activity of IO HSCs. Notably, genes encoding components of the mitophagy machinery were downregulated in IO BThal HSCs, further denoting the accumulation of damaged mitochondria.

According to previous publications, quiescent MMP^{low} HSCs that display low energy requirements, depend on glycolysis, whereas active MMP^{high} HSCs enhance both glycolysis and OXPHOS to meet their increased energy demands.[16,18,41-44] Our data confirm this heterogeneity within HSCs but assess that IO HSCs are predominantly within the MMP^{low} fraction. By coupling the cell cycle status with mitochondrial activity, we showed that in IO conditions, a fraction of MMP^{low} HSCs is more activated and iron is a potent stimulus for HSC activation. Previous work from our group, and others, showed a reduced stemness signature and self-renewal of HSCs in IO models,[11,13,24,25,29] which is consistent with their more active state. Lower total ATP in IO HSCs is suggestive of a more rapid consumption, which correlates well with their higher cycling activity.

Active IO HSCs showed uncoupled OXPHOS leading to reduced OXPHOS-derived ATP and restricted ability to

Figure 6 (continued) of TMRE is reported. Data are expressed relative to *th3* (n = 5). If not specified otherwise, data are presented as mean ± SEM. Significance indicated as $^{**}P < .01$; $^{*}P < .05$ was calculated using Kruskal-Wallis test for panels B-E, or Mann-Whitney test for panels G-J. WBM, whole bone marrow.

enhance mitochondrial respiration in response to stress. Furthermore, we performed untargeted metabolomic analysis revealing a downregulation of citrate, the metabolite generated in the first reaction of TCA cycle. The downstream TCA metabolites, isocitrate, oxalosuccinate, and 2-oxoglutarate, were upregulated in IO HSPCs, whereas succinate, fumarate, and malate were downregulated. These findings might indicate that the TCA cycle runs in reverse (reductive TCA cycle) to produce acetyl coenzyme A for fatty acid synthesis,[45] rather than running in the classic forward direction to generate ATP through OXPHOS.

The increase in glycolysis sustains actively proliferating HSCs with mitochondrial dysfunction and ineffective OXPHOS, as demonstrated by enhanced glucose uptake, upregulation of glycolytic enzymes (ie, *Tpi1*, *Gapdh*, and *Pklr*), and higher accumulation of glycolytic metabolites. Also, low intracellular content of lactate might suggest increased lactate consumption or extrusion in the extracellular space.[36] The behavior of IO HSCs, which proliferate despite glycolysis dependency, has been observed previously in rapidly proliferating cells that rely on aerobic glycolysis (Warburg effect) both in pathological (ie, cancer[46] and inflammation[47]) and physiological conditions (ie, HSPC aging,[48] T-cell activation[49]).

In patients affected by BThal and SCD, IO resulting from chronic hemolytic anemia, ineffective erythropoiesis, and therapeutic blood transfusions, is one of the main complications leading to multiple organ damage.[23,50,51] Although several iron chelators are available,[52,53] IO in organs is difficult to resolve once established. The efficacy of currently available chelation agents in the BM and HSCs has not been investigated; however, patients with iron-chelated BThal still display iron accumulation in the BM.[26] Thus, the identification of new therapeutic targets to reduce the effects of iron accumulation is needed.

Beyond defective erythropoiesis, BThal and SCD BM harbor HSCs with impaired functions[24,25,27] and we identified iron as a key contributor. HSCs and the BM niche are central elements in therapeutic HSC transplantation, both allogeneic and autologous in the setting of gene therapy, for several genetic blood disorders, including BThal and SCD.[21,54,55] Here, we demonstrated that IO-derived mtROS can be targeted to improve HSC frequency, quiescence, and self-renewal, which are essential features promoting the successful outcome of autologous transplantation in gene therapy. The depletion of IO-derived mtROS is sufficient to restore mitochondrial activity and reduce glycolysis dependency, highlighting the essential role of OXPHOS in preserving HSC function.[56,57]

The validation of these results in human cells and the understanding of the molecular mechanisms that lead to intracellular IO in HSCs are required for potential clinical translation. Overall, our findings bring new insights into the effects of IO in diseases and pave the way toward potential treatment to preserve HSC function in the context of transplantation.

Acknowledgments

The authors thank the Flow Cytometry Resource, Advanced Cytometry Technical Applications Laboratory at Ospedale San Raffaele for cell sorting; Cesare Covino, Maria Carla Panzeri, and Emanuele Colombo from the Advanced Light and Electron Microscopy BioImaging Center for electron microscopy analyses and immunofluorescence analyses; Federica Cugnata from the University Centre of Statistics in the Biomedical Sciences at Vita-Salute San Raffaele University for help with the statistical analyses; and the Harvard Center for Mass Spectrometry for untargeted metabolomics analyses.

This work was supported by Telethon Foundation (San Raffaele-Telethon Institute for Gene Therapy core grant 2021 to G.F and A.A.) and European Commission (Horizon Grant 2022-EDITSCD to G.F.). A.A is supported by the American Society of Hematology (2021 ASH Global Research Award) and by Cariplo Foundation (Young Researcher Grant 2022-0409).

Authorship

Contribution: S.S. designed the experimental work, performed the research, provided project coordination, wrote the manuscript, and analyzed, interpreted, and discussed data; L.C. and A.B. provided key reagents, designed the experimental work, and discussed data; M.R.L. designed the experimental work and discussed data; S.B. and I.M. performed bioinformatic analysis on the RNA-sequencing (RNA-seq) data; D.S. performed bioinformatic analysis on the metabolomics data; M.S. contributed to experimental work; C.M. and T.A.K. contributed to the metabolomics experiment; D.T.S. discussed data; A.A. performed RNA-seq and metabolomics experiments, provided project coordination, contributed to the study design, discussed data, and edited and critically reviewed the manuscript; G.F. supervised the project, provided coordination, obtained financial support, discussed data, and wrote and critically reviewed the manuscript; and all authors approved the final version of the manuscript.

Conflict-of-interest disclosure: T.A.K. is currently employed by Tessera Therapeutics. All the other authors declare no competing financial interests.

ORCID profiles: S.S., 0009-0005-9050-7853; M.R.L., 0000-0003-3413-8414; S.B., 0000-0003-4375-004X; C.M., 0000-0002-5755-1458; D.T.S., 0000-0001-9821-7133; I.M., 0000-0003-3587-3680; A.A., 0000-0001-6019-1345; G.F., 0000-0003-0790-3133.

Correspondence: Giuliana Ferrari, San Raffaele Telethon Institute for Gene Therapy, IRCCS San Raffaele Scientific Institute, Via Olgettina 58, 20132 Milan, Italy; email: ferrari.giuliana@hsr.it; and Annamaria Aprile, San Raffaele Telethon Institute for Gene Therapy, IRCCS San Raffaele Scientific Institute, Via Olgettina 58, 20132 Milan, Italy; email: aprile.annamaria@hsr.it.

Footnotes

Submitted 9 September 2025; accepted 2 March 2026; prepublished online on *Blood* First Edition 24 March 2026. https://doi.org/10.1182/blood.2025031552.

*A.A. and G.F. are joint last authors.

Metabolomic data for this study have been deposited in the MetaboLights database (study number MTBLS11778; https://www.ebi.ac.uk/metabolights/editor/study/MTBLS11778/descriptors).

Gene expression RNA-sequencing data for this study have been deposited in the European Nucleotide Archive database (accession number PRJEB31882; http://www.ebi.ac.uk/ena/data/view/PRJEB31882).

Original data are available from the corresponding authors, Giuliana Ferrari (ferrari.giuliana@hsr.it) and Annamaria Aprile (aprile.annamaria@hsr.it), on request.

The online version of this article contains a data supplement.

There is a *Blood* Commentary on this article in this issue.

The publication costs of this article were defrayed in part by page charge payment. Therefore, and solely to indicate this fact, this article is hereby marked "advertisement" in accordance with 18 USC section 1734.

REFERENCES

1. Laurenti E, Gottgens B. From haematopoietic stem cells to complex differentiation landscapes. *Nature*. 2018; 553(7689):418-426.
2. Nakamura-Ishizu A, Matsumura T, Stumpf PS, et al. Thrombopoietin metabolically primes hematopoietic stem cells to megakaryocyte-lineage differentiation. *Cell Rep*. 2018;25(7), 1772.e6-1785.e6.
3. Pietras EM, Mirantes-Barbeito C, Fong S, et al. Chronic interleukin-1 exposure drives haematopoietic stem cells towards precocious myeloid differentiation at the expense of self-renewal. *Nat Cell Biol*. 2016; 18(6):607-618.
4. Mitchell CA, Verovskaya EV, Calero-Nieto FJ, et al. Stromal niche inflammation mediated by IL-1 signalling is a targetable driver of haematopoietic ageing. *Nat Cell Biol*. 2023; 25(1):30-41.
5. Batsivari A, Haltalli MLR, Passaro D, Pospori C, Lo Celso C, Bonnet D. Dynamic responses of the haematopoietic stem cell niche to diverse stresses. *Nat Cell Biol*. 2020; 22(1):7-17.
6. Schonberger K, Obier N, Romero-Mulero MC, et al. Multilayer omics analysis reveals a non-classical retinoic acid signaling axis that regulates hematopoietic stem cell identity. *Cell Stem Cell*. 2022;29(1): 131.e10-148.e10.
7. Bigarella CL, Liang R, Ghaffari S. Stem cells and the impact of ROS signaling. *Development*. 2014;141(22):4206-4218.
8. Wang CY, Babitt JL. Liver iron sensing and body iron homeostasis. *Blood*. 2019;133(1): 18-29.
9. Kajarabille N, Latunde-Dada GO. Programmed cell-death by ferroptosis: antioxidants as mitigators. *Int J Mol Sci*. 2019;20(19):4968.
10. Kao YR, Chen J, Kumari R, et al. An iron rheostat controls hematopoietic stem cell fate. *Cell Stem Cell*. 2024;31(3): 378.e12-397.e12.
11. Muto Y, Nishiyama M, Nita A, Moroishi T, Nakayama KI. Essential role of FBXL5-mediated cellular iron homeostasis in maintenance of hematopoietic stem cells. *Nat Commun*. 2017;8:16114.
12. Zhao J, Jia Y, Mahmut D, et al. Human hematopoietic stem cell vulnerability to ferroptosis. *Cell*. 2023;186(4): 732.e16-747.e16.
13. Zhang D, Gao X, Li H, et al. The microbiota regulates hematopoietic stem cell fate decisions by controlling iron availability in bone marrow. *Cell Stem Cell*. 2022;29(2): 232.e7-247.e7.
14. Jin X, He X, Cao X, et al. Iron overload impairs normal hematopoietic stem and progenitor cells through reactive oxygen species and shortens survival in myelodysplastic syndrome mice. *Haematologica*. 2018;103(10):1627-1634.
15. Morganti C, Cabezas-Wallscheid N, Ito K. Metabolic regulation of hematopoietic stem cells. *Hemasphere*. 2022;6(7):e740.
16. Bartram J, Filippi MD. The new metabolic needs of hematopoietic stem cells. *Curr Opin Hematol*. 2022;29(4):188-193.
17. Filippi MD, Ghaffari S. Mitochondria in the maintenance of hematopoietic stem cells: new perspectives and opportunities. *Blood*. 2019;133(18):1943-1952.
18. Liang R, Arif T, Kalmykova S, et al. Restraining lysosomal activity preserves hematopoietic stem cell quiescence and potency. *Cell Stem Cell*. 2020;26(3): 359.e7-376.e7.
19. Qiu J, Gjini J, Arif T, Moore K, Lin M, Ghaffari S. Using mitochondrial activity to select for potent human hematopoietic stem cells. *Blood Adv*. 2021;5(6):1605-1616.
20. Kato GJ, Piel FB, Reid CD, et al. Sickle cell disease. *Nat Rev Dis Primers*. 2018;4:18010.
21. Kattamis A, Kwiatkowski JL, Aydinok Y. Thalassaemia. *Lancet*. 2022;399(10343): 2310-2324.
22. Lidonnici MR, Chianella G, Mende N, et al. Imbalanced TGFβ signalling and autophagy drive erythroid priming of hematopoietic stem cells in beta-thalassemia. *Nat Commun*. 2025;16(1):5639.
23. Aprile A, Sighinolfi S, Raggi L, Ferrari G. Targeting the hematopoietic stem cell niche in beta-thalassemia and sickle cell disease. *Pharmaceuticals (Basel)*. 2022;15(5):592.
24. Aprile A, Gulino A, Storto M, et al. Hematopoietic stem cell function in β-thalassemia is impaired and is rescued by targeting the bone marrow niche. *Blood*. 2020;136(5):610-622.
25. Aprile A, Raggi L, Bolamperti S, et al. Inhibition of FGF23 is a therapeutic strategy to target hematopoietic stem cell niche defects in β-thalassemia. *Sci Transl Med*. 2023;15(698):eabq3679.
26. Crippa S, Rossella V, Aprile A, et al. Bone marrow stromal cells from β-thalassemia patients have impaired hematopoietic supportive capacity. *J Clin Invest*. 2019; 129(4):1566-1580.
27. Tang A, Strat AN, Rahman M, et al. Murine bone marrow mesenchymal stromal cells have reduced hematopoietic maintenance ability in sickle cell disease. *Blood*. 2021; 138(24):2570-2582.
28. Park SY, Matte A, Jung Y, et al. Pathologic angiogenesis in the bone marrow of humanized sickle cell mice is reversed by blood transfusion. *Blood*. 2020;135(23): 2071-2084.
29. Javazon EH, Radhi M, Gangadharan B, Perry J, Archer DR. Hematopoietic stem cell function in a murine model of sickle cell disease. *Anemia*. 2012;2012:387385.
30. Chai X, Li D, Cao X, et al. ROS-mediated iron overload injures the hematopoiesis of bone marrow by damaging hematopoietic stem/progenitor cells in mice. *Sci Rep*. 2015; 5:10181.
31. Mansell E, Sigurdsson V, Deltcheva E, et al. Mitochondrial potentiation ameliorates age-related heterogeneity in hematopoietic stem cell function. *Cell Stem Cell*. 2021;28(2): 241.e6-256.e6.
32. Kiel MJ, Yilmaz OH, Iwashita T, Yilmaz OH, Terhorst C, Morrison SJ. SLAM family receptors distinguish hematopoietic stem and progenitor cells and reveal endothelial niches for stem cells. *Cell*. 2005;121(7): 1109-1121.
33. Oguro H, Ding L, Morrison SJ. SLAM family markers resolve functionally distinct subpopulations of hematopoietic stem cells and multipotent progenitors. *Cell Stem Cell*. 2013;13(1):102-116.
34. Kakhlon O, Cabantchik ZI. The labile iron pool: characterization, measurement, and participation in cellular processes(1). *Free Radic Biol Med*. 2002;33(8): 1037-1046.
35. Riedelberger M, Kuchler K. Analyzing the quenchable iron pool in murine macrophages by flow cytometry. *Bio Protoc*. 2020;10(6):e3552.
36. Ippolito L, Morandi A, Giannoni E, Chiarugi P. Lactate: a metabolic driver in the tumour landscape. *Trends Biochem Sci*. 2019;44(2):153-166.
37. Youle RJ, van der Bliek AM. Mitochondrial fission, fusion, and stress. *Science*. 2012; 337(6098):1062-1065.
38. Twig G, Shirihai OS. The interplay between mitochondrial dynamics and mitophagy. *Antioxid Redox Signal*. 2011;14(10): 1939-1951.
39. Ito K, Hirao A, Arai F, et al. Reactive oxygen species act through p38 MAPK to limit the lifespan of hematopoietic stem cells. *Nat Med*. 2006;12(4):446-451.
40. Ryan TM, Ciavatta DJ, Townes TM. Knockout-transgenic mouse model of sickle cell disease. *Science*. 1997;278(5339): 873-876.
41. Chen C, Liu Y, Liu R, et al. TSC-mTOR maintains quiescence and function of hematopoietic stem cells by repressing mitochondrial biogenesis and reactive oxygen species. *J Exp Med*. 2008;205(10): 2397-2408.
42. Vannini N, Girotra M, Naveiras O, et al. Specification of haematopoietic stem cell fate via modulation of mitochondrial activity. *Nat Commun*. 2016;7:13125.
43. Takubo K, Nagamatsu G, Kobayashi CI, et al. Regulation of glycolysis by Pdk functions as a metabolic checkpoint for cell cycle quiescence in hematopoietic stem cells. *Cell Stem Cell*. 2013;12(1):49-61.
44. Ito K, Turcotte R, Cui J, et al. Self-renewal of a purified Tie2+ hematopoietic stem cell population relies on mitochondrial clearance. *Science*. 2016;354(6316):1156-1160.

45. Berg JM, Tymoczko JL, Gatto GJ Jr, Stryer L. *Biochemistry*. 8th ed. WH Freeman & Company; 2015.

46. Vander Heiden MG, Cantley LC, Thompson CB. Understanding the Warburg effect: the metabolic requirements of cell proliferation. *Science*. 2009;324(5930):1029-1033.

47. Rodriguez-Prados JC, Través PG, Cuenca J, et al. Substrate fate in activated macrophages: a comparison between innate, classic, and alternative activation. *J Immunol*. 2010;185(1):605-614.

48. Hennrich ML, Romanov N, Horn P, et al. Cell-specific proteome analyses of human bone marrow reveal molecular features of age-dependent functional decline. *Nat Commun*. 2018;9(1):4004.

49. Macintyre AN, Gerriets VA, Nichols AG, et al. The glucose transporter Glut1 is selectively essential for CD4 T cell activation and effector function. *Cell Metab*. 2014;20(1):61-72.

50. Rivella S. Iron metabolism under conditions of ineffective erythropoiesis in β-thalassemia. *Blood*. 2019;133(1):51-58.

51. Vinchi F, Sparla R, Passos ST, et al. Vasculotoxic and pro-inflammatory action of unbound haemoglobin, haem and iron in transfusion-dependent patients with haemolytic anaemias. *Br J Haematol*. 2021;193(3):637-658.

52. Taher AT, Saliba AN. Iron overload in thalassemia: different organs at different rates. *Hematol Am Soc Hematol Educ Program*. 2017;2017(1):265-271.

53. Coates TD, Wood JC. How we manage iron overload in sickle cell patients. *Br J Haematol*. 2017;177(5):703-716.

54. Telen MJ, Malik P, Vercellotti GM. Therapeutic strategies for sickle cell disease: towards a multi-agent approach. *Nat Rev Drug Discov*. 2019;18(2):139-158.

55. Lidonnici MR, Scaramuzza S, Ferrari G. Gene therapy for hemoglobinopathies. *Hum Gene Ther*. 2023;34(17-18):793-807.

56. Anso E, Weinberg SE, Diebold LP, et al. The mitochondrial respiratory chain is essential for haematopoietic stem cell function. *Nat Cell Biol*. 2017;19(6):614-625.

57. Bejarano-Garcia JA, Millán-Uclés Á, Rosado IV, et al. Sensitivity of hematopoietic stem cells to mitochondrial dysfunction by SdhD gene deletion. *Cell Death Dis*. 2016;7(12):e2516.